Transport analysis in an electron cyclotron heating power scan of TJ-II plasmas

2014 Plasma Phys. Control. Fusion 56 075024

(http://iopscience.iop.org/0741-3335/56/7/075024)

IOP Publishing Plasma Physics and Controlled Fusion

Plasma Phys. Control. Fusion **56** (2014) 075024 (10pp) doi:10.1088/0741-3335/56/7/075024

Transport analysis in an electron cyclotron heating power scan of TJ-II plasmas

S Tallents[1], D López-Bruna[2], J L Velasco[2], M A Ochando[2], B Ph Van Milligen[2], V I Vargas[1], J J Martinell[3], D Tafalla[2], J M Fontdecaba[2], J Herranz[2], E Blanco[2], F L Tabarés[2], T Estrada[2], I Pastor[2] and The TJ-II Team

[1] Instituto Tecnológico de Costa Rica, Cartago, Costa Rica
[2] Asociación EURATOM-CIEMAT, Madrid, Spain
[3] Instituto de Ciencias Nucleares (UNAM), México D.F., México

Received 16 December 2013, revised 23 April 2014
Accepted for publication 16 May 2014
Published 19 June 2014

Abstract

The response of transport in low density (line average $\bar{n} \approx 0.6 \times 10^{19}\,\mathrm{m}^{-3}$) plasmas to electron cyclotron resonance heating (ECH) power, $100\,\mathrm{kW} \lesssim Q_{\mathrm{ECH}} \lesssim 400\,\mathrm{kW}$, is documented for the TJ-II Heliac-type stellarator. Radially resolved electron heat balance shows no significant differences between boron or lithium coating of the vacuum chamber walls. The main trends in electron heat transport are found to be similar to other stellarator/heliotron devices and are compatible with neoclassical calculations in the bulk of the plasma. According to our calculations the heat fluxes are anomalous near the edge, $\rho \gtrsim 0.8$ where ρ is the normalized minor radius, but the uncertainties there are large. Particle transport in the density gradient region, $\rho \approx 0.8$, has little sensitivity to the variation of heating power and is compatible with neoclassical predictions. Neoclassical transport of particles and electron heat is found to be dominant in the gradient regions of typical ECH plasmas of the TJ-II Heliac.

Keywords: plasma physics, heat transport, stellarator, TJ-II, neoclassical

(Some figures may appear in colour only in the online journal)

1. Introduction

A common feature of both tokamak and stellarator plasmas is power degradation of confinement, quantified in the latter case in the empirical ISS04 scalings [1]. Much work on helical devices in the 1990s was devoted to general transport studies; establishing that this degradation is linked to heating power and the heat losses in the electron channel are strongly anomalous (see [2] and references therein); and that many features of transport are shared with tokamaks [3], thus making stellarator transport studies extensible to the physics of tokamak transport. An important area of research specific to stellarators is that collisional transport is strongly dependent on the radial electric field and, moreover, able to explain general experimental results [4]. Therefore, even if the transport is dominantly anomalous in some plasma conditions, the collisional radial particle fluxes may still lead the confinement trends and the establishment of radial electric fields and sheared $E \times B$ flows [5], which also affect turbulent transport. Thus the evaluation of collisional fluxes remains as important a task [6] as it has been in the past (see, for example, [7]).

Global confinement studies on TJ-II electron cyclotron heating (ECH) discharges under boronized wall conditions exhibit power degradation, with energy confinement time scaling as $\tau_{\mathrm{E}} \sim Q_{\mathrm{ECH}}^{-0.6}$ [8]. The lithiumization of the vacuum chamber walls [9] has considerably extended the operation of higher density neutral beam injection (NBI) plasmas—n_{e} about 2–$5 \times 10^{19}\,\mathrm{m}^{-3}$, $T_{\mathrm{e}} \approx 0.3\,\mathrm{keV}$, $T_{\mathrm{i}} \approx 0.15\,\mathrm{keV}$, where particle control is critical—but has had no impact in the confinement properties of ECH plasmas—$n_{\mathrm{e}} < 10^{19}\,\mathrm{m}^{-3}$, $T_{\mathrm{e}} \approx 1\,\mathrm{keV}$, $T_{\mathrm{i}} \approx 0.1\,\mathrm{keV}$—beyond improved density control via gas puffing through lower recycling [10, 11]. On the other hand, local confinement studies have investigated the variation of effective electron heat diffusivity $\chi_{\mathrm{e}}^{\mathrm{eff}}$ in the range of normalized radius 0.2–0.8 as a function of rotational transform, density and ECH

power (Q_{ECH}) in boronized wall plasmas [12]; in that study the density dependence of $\chi_{\mathrm{e}}^{\mathrm{eff}}$ was found to obey a power law with the exponent varying with radius in the mid-plasma, though no significant dependence in the core was observed. In terms of heating power, only three heating power scenarios were investigated: Q_{ECH} of 200, 300 and 400 kW, resulting in large standard errors due to the relatively few repeat discharges available. The effective $\chi_{\mathrm{e}}^{\mathrm{eff}}$ was seen to increase with deposited heat—broadly doubling as Q_{ECH} was increased from 200 to 400 kW—and the presence of low order rational magnetic surfaces was found to locally modify the electron heat transport.

Generally speaking, transport in the main body of TJ-II ECH discharges shows similarities to equivalent scenarios in other devices: relatively low, flat density and ion-temperature profiles; peaked electron temperature profiles T_{e}, and weak collisional coupling between ions and electrons, $T_{\mathrm{i}} \ll T_{\mathrm{e}}$. Core collisionalities in these low collisionality plasmas are $\nu_{\mathrm{e}}^{*} \sim 10^{-3}$–$10^{-4}$ and $\nu_{\mathrm{i}}^{*} \sim 10^{-1}$ (see figure 1 in [6]). Neverthless, although the contributions of the $\frac{1}{\nu}$ are expected to be important, giving $Q \sim T^{\frac{2}{7}}$; a strongly positive E_r can improve the energy content in the core plasma by decreasing neoclassical heat transport [13] in a phenomenon referred to as Core Electron Root Confinement (CERC) [4]: the electrons may be in the $\sqrt{\nu}$ regime, where the scaling is only $Q \sim T^{\frac{5}{4}}$. In this case the electric field is generated as one of the solutions satisfying the ambipolar condition for neoclassical particle fluxes and represents a good practical example of the link between collisional transport and electric fields in stellarators. However it is also known that any additional non-ambipolar fluxes may participate in determining E_r. For example, in W7-AS the ECH-driven convective flux of supra-thermal ripple-trapped electrons is found to play the dominant role in the generation of strongly positive E_r [14, 15]. Another such phenomenon in TJ-II, toroidal radiation asymmetry phase or TRAP, has been linked to the convective flux of superthermal electrons driven by ECH heating power and related to the presence of rational surfaces in the plasma [16], which are clear contributors to the CERC phenomenon in the TJ-II [17, 18]. Additionally, a threshold for fast electron losses and particle confinement was found that depends on line averaged density in TJ-II discharges with fixed ECH power [19]. It is then clear that any mechanism able to unbalance electron and ion radial fluxes can exert a strong influence on E_r and thus on transport. The heating and the magnetic topology can be at least partly controlled externally while the collisional transport in a given magnetic confinement geometry is intrinsic to the plasma parameters. As neoclassical theory has a robust foundation, a thorough documentation of the extent of its compatibility with experimental results can help to assess the role of electric fields as internal or (possibly) external confinement modifiers.

First works on the comparison between neoclassical and experimental fluxes in TJ-II plasmas were undertaken to investigate the phenomenon later referred to as CERC under metallic wall conditions, paying particular attention to the core plasma. ECH discharges from a small set of discharges at different densities were fitted and analyzed, establishing a comparison between the power balance and neoclassical calculations in the core [13]. The reduced set of profiles could not account for their experimental variability. Reference [12] showed a systematic study of balance electron heat transport on boronized-wall ECH plasmas; however the impact of heating power could not be fully resolved from the variation in $\chi_{\mathrm{e}}^{\mathrm{eff}}$ generated by the other variables under consideration. The work presented here focuses on extending the study to achieve a better understanding of the dependency of the radial electron heat fluxes on Q_{ECH} by increasing the resolution of the scan; increasing the number of discharges performed for each scenario; and extending the parameter scan into lithium wall conditions. Additionally, an evaluation of particle transport in the density gradient region is presented and both transport branches—electron heat and particles—are compared with neoclassical predictions.

We start the paper with brief descriptions of the TJ-II device, the diagnostics used in this work and the experiments performed (section 2); and the tools used for the analysis (section 3). Section 4 is devoted to transport analysis: firstly we show the results of heat and particle balance, then we compare these results with those from the neoclassical calculations. A summary of the results and the conclusions are finally presented in section 5.

2. Experiments and diagnostics

The results presented were obtained in TJ-II ECH plasmas using hydrogen as a working gas in discharges with boronized or lithiumized first wall. TJ-II is a helical, 4-period, low magnetic shear device; with major radius $R = 1.5$ m and average minor radius $a \approx 0.2$ m; and magnetic field strength at the magnetic axis $B_0 \approx 1$ T. The plasmas were heated by ECH 2nd harmonic at 53.2 GHz with X-mode polarization and a plasma density cut-off value of 1.75×10^{19} m^{-3} corresponding to line averaged densities around 1.2×10^{19} m^{-3}. The microwaves are generated with two gyrotrons, set up in this case for on-axis heating and 300 kW maximum nominal power each. Port-through power is estimated at 85% of nominal heating power, with 70% of port-through power subsequently absorbed by the plasma [8], meaning deposited ECH power (Q_{ECH} hereonout refers to deposited ECH heating power) is 60% of nominal ECH power. Only the TJ-II standard magnetic configuration was used ($1.56 \leqslant \iota/2\pi \leqslant 1.65$, plasma volume $\approx$1 m^3), which has the vacuum magnetic resonance $\iota/2\pi = 8/5$ around $\rho = r/a = 0.8$. Here r is the average minor radius of flux surfaces, which enclose a plasma volume $\propto r^2$.

TJ-II is a limiter machine with its last closed flux surface (LCFS) defined by either its two movable graphite poloidal limiters or by its helical one. The discharges selected for this study had the mobile limiters at or outside the LCFS, so the long helical limiter, which protects the central (helical and circular) coils, becomes the main plasma-wall interaction zone. Gas puffing rates and H_α intensity signals in three different sectors (poloidal limiter, helical limiter in two different toroidal sectors) have been recorded during the discharges.

35 discharges were selected for analysis: those in steady state, with variation in line averaged density ($\bar{n}_{\mathrm{e}}$) less than 0.04×10^{19} m^{-3} in the 10 ms period centered on the Thomson scattering (TS) diagnostic [20]. Ten discharges had boronized

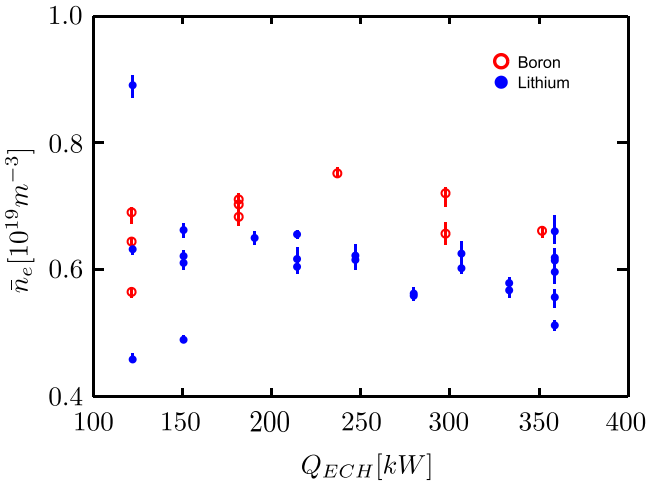

Figure 1. $\bar{n}_e$ and nominal ECH power at the Thomson time, showing the parameter space explored in investigation. Boron coated wall conditions are shown by red circles and lithium coated wall conditions are shown by blue dots.

(B) wall conditions and 25 discharges to lithiumized (Li) wall conditions. The parameter space in $\bar{n}_e$ and Q_{ECH} explored is shown in figure 1.

Radial electron temperature (T_e) and density (n_e) profiles up to $\rho \approx 0.75$ were obtained from TS. T_e and n_e in the edge region ($\rho \gtrsim 0.7$) were obtained using information from the helium beam diagnostic [21] where available. The respective profiles were composed from the combined diagnostic information using Bayesian inference methods [22].

The central ion temperature, $T_{i0} = T_i(\rho = 0.1)$, is obtained by a charge exchange (CX) neutral particle analyzer for all shots [23]. T_i profiles in TJ-II ECH plasmas are similar to the density profiles and with edge values smaller than the corresponding electron temperatures [24, 25]. Therefore we have taken ion temperature profiles in the form

$$T_i(\rho) = \frac{T_{i0}}{n_0}[n(\rho) - \rho n_a] + \frac{1}{2}\rho T_{ea}$$

where $T_{ea} = T_e(\rho = 1.0)$ and $n_a = n(\rho = 1.0)$ which guarantees a similarity with the density profile with the proper core value of the ion temperature, T_{i0}, while the edge value is forced to half the electron one, $(1/2)T_{ea}$. For all shots, line averaged density through the magnetic axis is obtained from microwave interferometry.

Temperature data from the various diagnostics can be seen in figure 2(*a*) where we show the values of core T_i (errors $<10\%$) and edge T_e from the helium beam for the shots selected for analysis. In figure 2(*b*) we plot the electron temperatures at different radii for each of the boronized and lithiumized wall condition sets, again sorted by ECRH power. To better illustrate the plasma conditions in this work, figure 3 shows average density and electron temperature profiles for each heating power, with error bars showing the extreme cases.

Finally, for 19 of the Li-coated wall discharges a radial profile of electrostatic potential (ϕ) was measured using the 125 keV Cs^+ heavy ion beam probe. Generally speaking, all the plasmas used for the neoclassical comparison show positive electric field values for $\rho < 0.6$ with a maximum $E_r \sim 5\,\mathrm{kV\,m^{-1}}$ around $\rho = 1/3$; while outside $\rho = 0.6$ the electric field has large errors $|\Delta E_r| \sim \pm 3\,\mathrm{kV\,m^{-1}}$ being in all cases compatible with zero. These are typical ECH plasmas of the TJ-II Heliac and the corresponding HIBP profiles are separately presented in [26]. As the measurements do not cover the full plasma radius, we choose here to use the E_r given by the ambipolarity of the neoclassical (NC) fluxes, which has been shown to be good enough for low density TJ-II plasmas [27]. For our transport analysis, the relevant feature is that our ECH plasmas have a relatively strong positive electric field in the core and small and negative close to the edge.

3. Transport analysis

Two basic tools have been used to interpret the experimental data: (i) steady state balance of heat and particles to obtain confinement times and experimental radial transport, and (ii) neoclassical transport calculations [28] based on the Drift Kinetic Equation Solver (DKES) [29].

The power balance analysis is carried out during the stationary phase of the discharges based on the experimental profiles of T_e and n_e, on CX and bolometry data, and on the absorbed heating power (see section 2) as in the global studies in [8]. All analysis is performed with the ASTRA shell [30] using vacuum flux surface metrics coefficients for the appropriate magnetic configuration. The main region of power deposition in TJ-II is known to occur inside $\rho = 0.2$, but the deposition region is subject to some variations with heating power due to the creation of electron super-thermal tails [31]. For simplicity the heating power density has been modeled for all nominal heating powers using a Gaussian-shaped deposition profile of width $\approx$0.3. This is a common assumption in balance analyses (e.g. [7, 32]) and eases the comparison with other devices and previous TJ-II works, although balance values in the deposition zone must be taken as indicative.

Radiation profiles have been considered where available, allowing us to confirm that the net radiation losses in these plasmas amount to at most 10% of the available heating power; it will be seen in the next section that including radiation does not make a major difference in the power balance analysis. Therefore, as the corresponding experimental information was not available for all the discharges in the scans, the study of transport balance is done without considering radiation profiles in order to perform a homogeneous analysis of the data set. The power balance includes collisional electron–ion energy transfer, although this is also quite small in TJ-II ECH plasmas. The experimental electron fluxes are expressed with dimensions of velocity,

$$Q_e^{\mathrm{eff}} = 625\frac{Q_e}{n_e T_e S}, \qquad (1)$$

where S ($\mathrm{m^2}$) is the magnitude of the LCFS and Q_e (MW) is the electron heat flux obtained in steady state as the volume integral of the ECRH and Coulomb heat exchange power density terms. Units for density and temperature are 10^{19} $\mathrm{m^{-3}}$ and keV respectively. In order to ease comparison with other works, we use effective diffusivities

$$\chi_e^{\mathrm{eff}} = L_{T_e} Q_e^{\mathrm{eff}} \qquad (2)$$

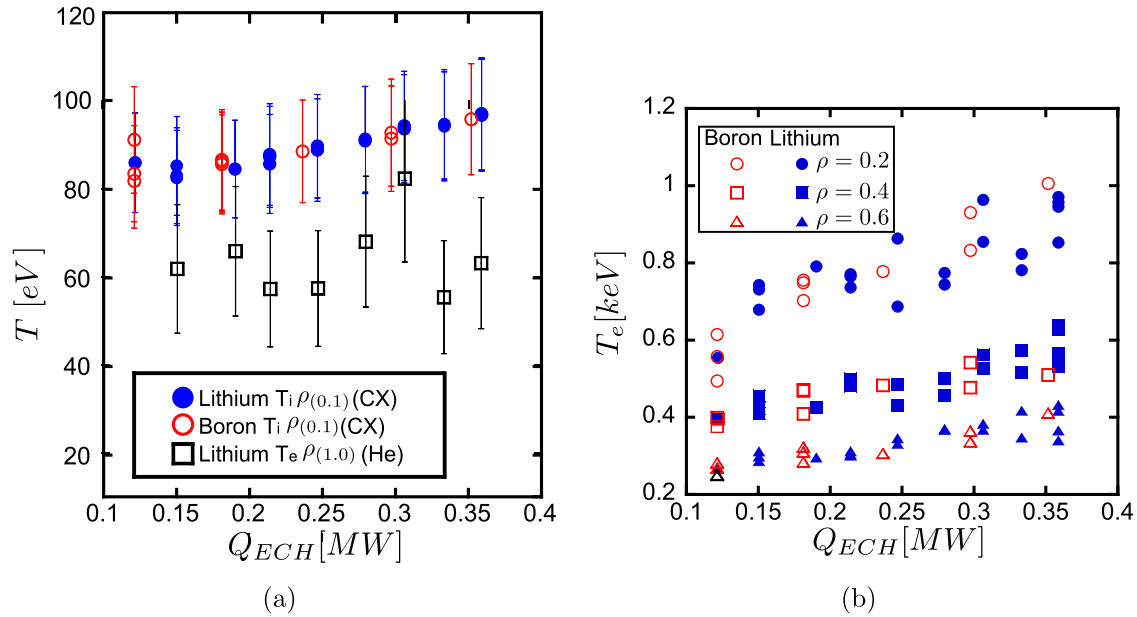

Figure 2. As a function of the absorbed heating power: (*a*) central ion temperature from CX spectroscopy measurements for lithium (solid blue circles) and boron (hollow red circles) wall conditions and helium beam diagnostic (black squares, lithium wall conditions only); (*b*) electron temperature from Thomson scattering diagnostics at three different normalized radii in boron (hollow) and lithium (solid) wall conditions; the diagnostic error bars (not drawn for clarity) are comparable to the data dispersion at each QECH.

related by the characteristic electron temperature gradient scale-length L_{T_e}. An analogous expression relates particle effective diffusivities and fluxes, $D_e^{\rm eff} = L_{n_e}\Gamma_e^{\rm eff}$. The corresponding neoclassical fluxes, $Q_e^{\rm neo}$ and $\Gamma_e^{\rm neo}$, are obtained also in m s^{-1} units from equations (2) and (3) in [28].

Particle balance analysis is based on calculations performed with the Monte-Carlo code Eirene [33] using an iterative method [19]. In brief, the method consists of calculating a self-consistent (i.e. compatible with steady state) particle source based on the plasma profiles, fueling efficiency and gas puffing data. Particle transport analysis is performed on the set of discharges with lithiumized wall, characterized by a small recycling factor that can be as low as ∼0.1. When lithiumization is not very fresh—as in our experimental conditions—the recycling coefficient rises to around 0.5 [9]. However the recycling from the wall is not known with precision and evolves depending on the number of discharges subsequent to the wall coating, glow discharge conditioning, the working gas and the performance of the coating itself. In consequence we expect some scatter in the net source and consequently confinement times. The fueling efficiency should be quite similar for plasmas operated with the same configuration and fueling technique, but its value—fixed to 75%—is simply based on the high efficiency found in this kind of discharge [9]. Therefore the calculations of the plasma particle sources will be used as an order-of-magnitude estimate of fluxes and effective particle transport coefficients to be compared with the neoclassical calculations.

Particle fluxes that reproduce the experimental profiles given the source profile are modeled with a transport coefficient and a flux averaged radial velocity, v_r, to represent convective contributions to the radial transport. This velocity term models the ECH pump-out as a drift on the order of a few m s^{-1} near the heating deposition zone and the radial particle drifts in the edge region. In the transport analysis we will compare the total fluxes from balance and NC, but we split balance calculations into diffusive and convective parts. The latter is based on non-local numerical estimates [19, 34] that yield radial drifts ∼10 m s^{-1}. The effective diffusion is calculated in terms of the integral of the electron source term $S_{\rm I}(\rho)$, the electron density profile, the radial drift v_r and metrics-related profiles,

$$D_e^{\rm eff}(\rho) = -\frac{S_I - V' n v_r\,|\langle\nabla\rho\rangle|}{V' n' \langle(\nabla\rho)^2\rangle}, \qquad (3)$$

so the estimated contribution from the above mentioned convective fluxes to the profile shape are removed to leave only the contribution from diffusion and any remaining anomalous processes. Here the derivative with respect to ρ is indicated with a prime. The flux surface average is indicated with $\langle\cdots\rangle$. Note that when $v_r = 0$ a standard formula for the effective diffusivity is obtained.

4. Experimental results from the ECH power scan

Lithium coating of the first wall has proven to be an effective technique for particle density control in NBI heated TJ-II plasmas [9], where edge temperatures are found to be significantly higher under Li than B wall conditioning. However, in ECH plasmas the edge electron temperature values are found to be comparable for the two wall coatings (see figure 2 and also [11] for further detail). As the core transport should not be affected by the wall coating unless the latter causes some systematic change in the profiles (e.g. through radiation losses), we start by looking for this change in the effective diffusivities $\chi_e \sim \frac{1}{n_e T_e}$ in the boron and lithium datasets. Once they are found equivalent, as will be shown,

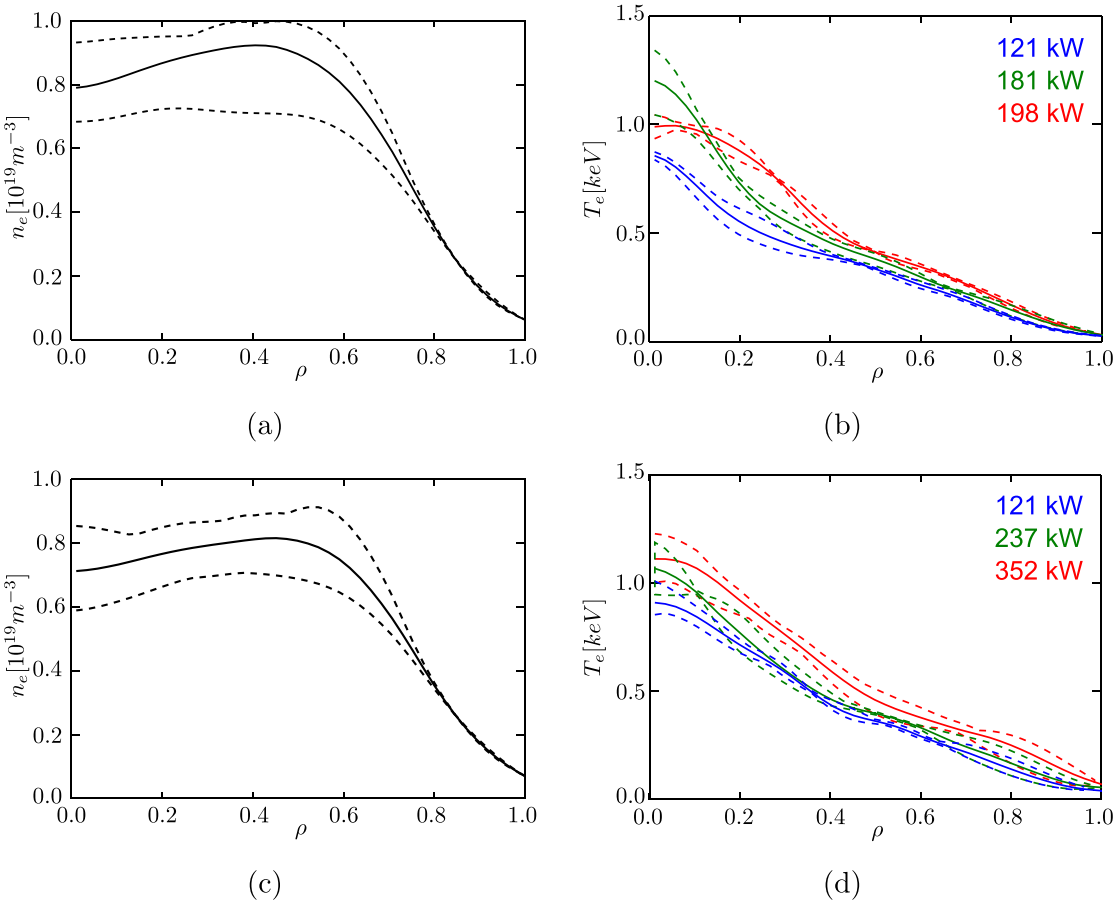

Figure 3. Average smoothed TS n_e profiles for boron (a) and lithium (c) coated wall conditions. Dashed lines show maximum and minimum values. Representative smoothed Thomson scattering T_e profiles recorded at three selected heating powers for boron (b) and lithium (d) coated wall conditions.

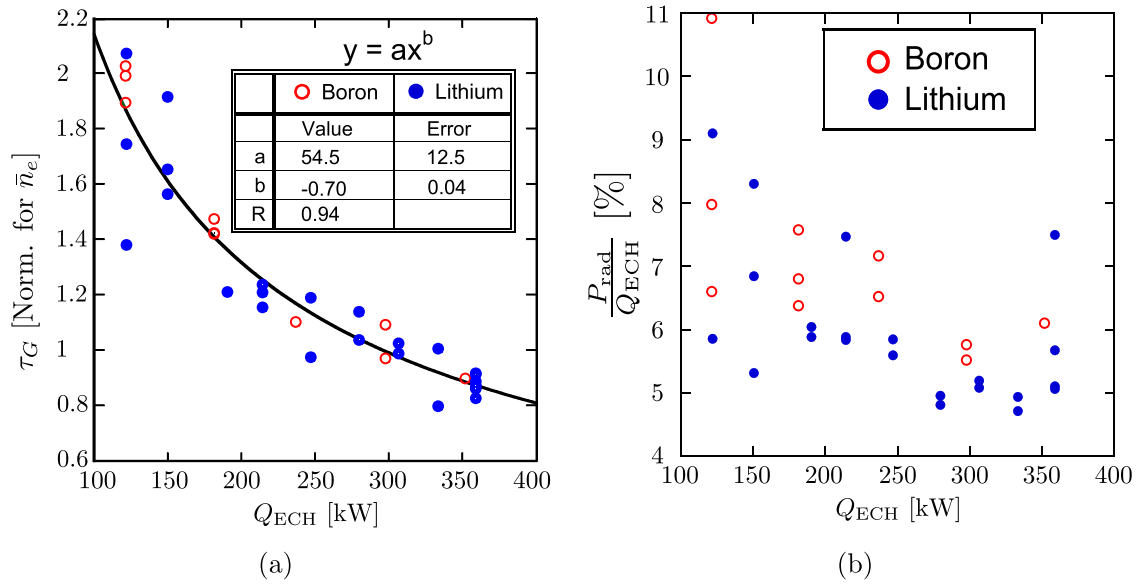

Figure 4. (a) Energy confinement times (unadjusted for radiation) τ_G versus heating power and (b) fraction of radiated power as a function of Q_{ECH} for boron (red hollow) and lithium (solid blue) conditioned walls.

they can be combined to make a comparison with neoclassical calculations independently of the wall coating.

Figure 4(a) shows the energy confinement time, τ_G, calculated using the absorbed ECH heating power (unadjusted for radiation losses) and stored energy for both boron and lithium walls at different ECH heating powers. The behavior shows power degradation consistent with the TJ-II scaling [8] for the boron wall conditions in both cases—please note that

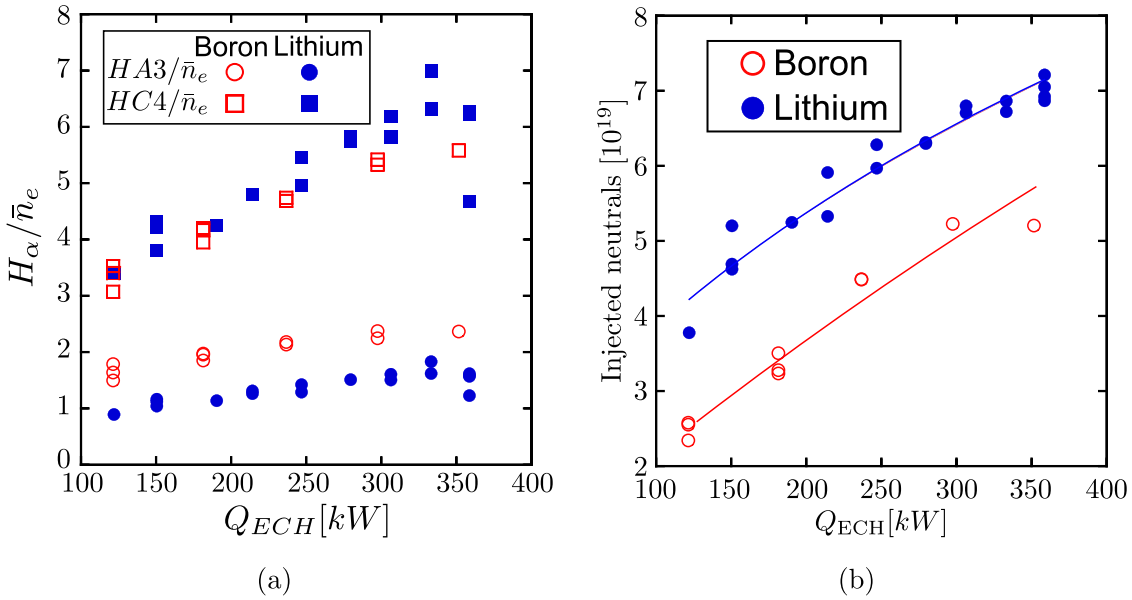

Figure 5. As a function of heating power: (*a*) intensity of the H_α signals (arbitrary units) divided by the line density around the time of the TS measurement for discharges belonging to the boron and lithium ECH power scan. Shown are H_α monitors looking at the poloidal (circles) and helical (squares) limiters in lithium (blue solid) and boronized (red hollow) wall plasmas. (*b*) Total injected neutral by valve until the Thomson time in boronized and Li-coated wall conditions.

in [8] a much larger dataset is handled. The energy confinement times show dependencies of the form $\tau_{\rm G} \sim Q_{\rm ECH}^{-0.61\pm0.06}$ and $\tau_{\rm G} \sim Q_{\rm ECH}^{-0.71\pm0.06}$ for boron and lithium conditioning respectively. The apparently larger values with boronized wall are a consequence of slightly larger densities in this case (figure 1). As the linear relationship between $\tau_{\rm G}$ and line density is reasonably well established [8] we have combined B and Li data after normalizing by the density using parameters in figure 4 of [35] to obtain a scaling law $\tau_{\rm G} \propto Q_{\rm ECH}^{-0.7\pm0.04}$. Radiated powers in both wall conditionings represent typically 5–8% of the deposited power and follow the expected behavior in these plasmas: proportionality with heating power and density (the latter explains the dispersion in the data). The (barely significant) higher radiated powers in the B case are most likely due to line emission from different impurity content. We therefore expect the same behavior of the effective diffusivities in both Li and B cases.

Global particle transport shows no essential difference between B and Li cases according to the intensity of the H_α light—normalized to the line density—emitted (figure 5(*a*)), although the puffing levels are significantly higher by a factor of 2 in the latter in order to obtain the same density (figure 5(*b*)), as noted in general for the lithium conditioning of the walls [9]. At first glance figure 5(*a*) indicates a progressive loss of confinement as the heating power is increased. In particular, the H_α signal labeled 'C4' collects light from a wide plasma zone interacting with the helical limiter, while signal labeled 'A3' collects light from a much smaller interaction area with the poloidal limiter. The poloidal limiter 'A3' was 2 cm away from the LCFS in the Li cases of figure 5(*a*), which explains why there is a smaller $H_\alpha/\bar{n}$ ratio in comparison with the boron cases. Aside from this, the signals from both limiters show an approximately linear increment with $Q_{\rm ECH}$. However, we should be aware that outgoing fluxes of thermal ions are not the only contribution to the H_α signals and that direct losses, which increase with $Q_{\rm ECH}$, also contribute. On the other hand, no significant trend with $Q_{\rm ECH}$ has been found in the calculation of particle confinement times, which instead yields scattered values of around $\tau_{\rm p} = 10 \pm 3$ ms. This is partly a consequence of the uncertainty of edge electron temperatures, which affect the estimated sources. Typical error bars in $T_{\rm ea}$ approach 30% (see figure 2). Experimental values for ECH plasmas in TJ-II are normally $5 \lesssim \tau_{\rm p} \lesssim 15$ ms [36], so we can use the calculated particle source profiles to obtain reasonable effective particle diffusivity profiles.

4.1. Effective diffusivities and flux profiles

Composite profiles of the electron heat flux (equation (1)) for each heating power have been constructed by averaging profiles obtained from individual shots with the same heating power. The results are shown in figures 6(*a*) (B) and 6(*c*) (Li). The respective figures 6(*b*) and 6(*d*) show the standard errors from the repetitions as a percentage of the corresponding flux. When converted to diffusivities (equation (2)), in the inner region ($0.20 < \rho < 0.30$) the values are as high as 2–3 $\rm m^2\,s^{-1}$ rising to 4–5 $\rm m^2\,s^{-1}$ when the power exceeds 300 kW. These values agree with those found earlier in TJ-II [13] and are typical of medium-size, non-optimized stellarators in the $1/\nu$ regime of collisionality (see, e.g., [5, 37]). In general it can be said that, within the range $0.2 \leqslant \rho \leqslant 0.8$, $\chi_{\rm e}^{\rm eff}$ peaks (although is barely significant) around $0.4 \lesssim \rho \lesssim 0.6$ corresponding to the change in gradient of the $T_{\rm e}$ profile (i.e. the foot of the $T_{\rm e}$ peak, see figure 3). Further out there is a region with very large values of the experimental fluxes (figure 6) and $\chi_{\rm e}^{\rm eff}$, as found in many other devices; for instance, $\chi_{\rm e}^{\rm eff} \sim \rho^6$ in Uragan 3-M plasmas [38]. These large fluxes reflect the low electron pressure near the plasma edge. Note, however,

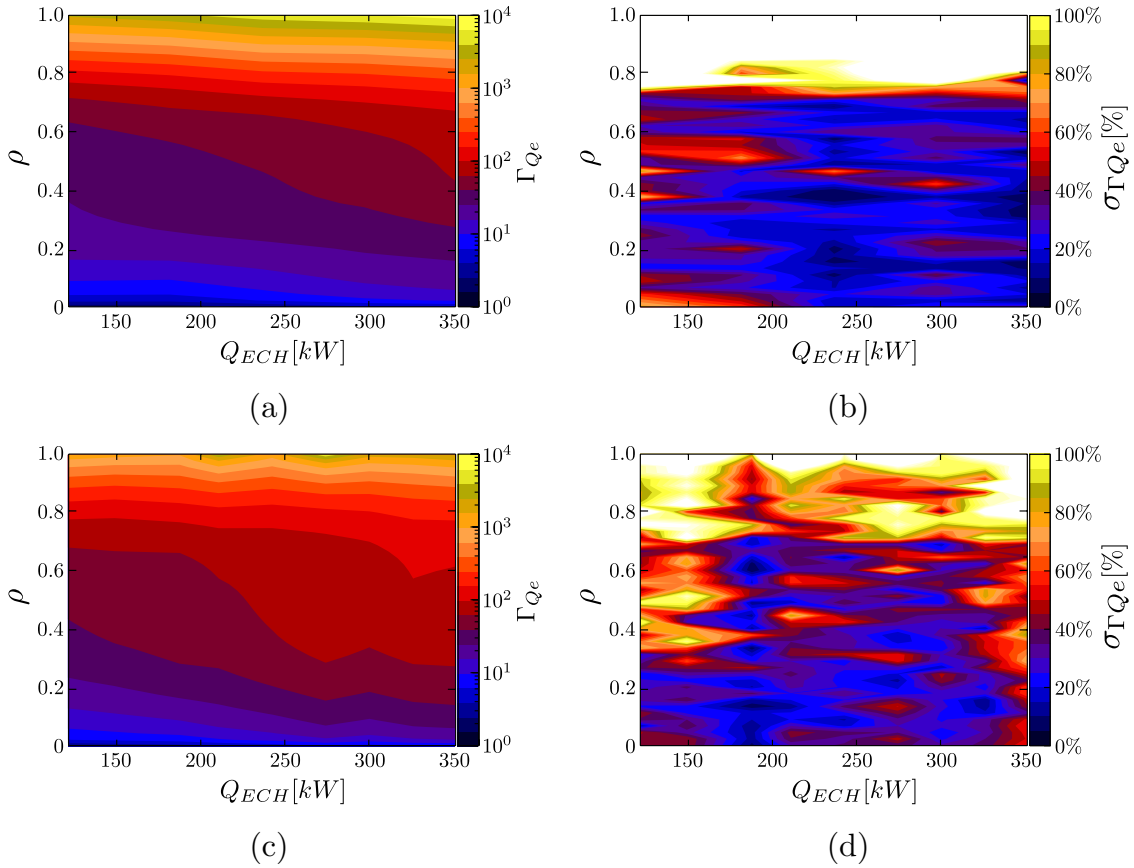

Figure 6. Contour maps of $\log_{10} Q_e^{\text{eff}}$ under (*a*) boron and (*c*) lithium wall conditions as a function of normalized radius and heating power; and standard error presented as a percentage in (*b*) and (*d*) respectively. Errors associated with the uncertainties in the power deposition profile ($\rho \lesssim 0.2$) are not considered.

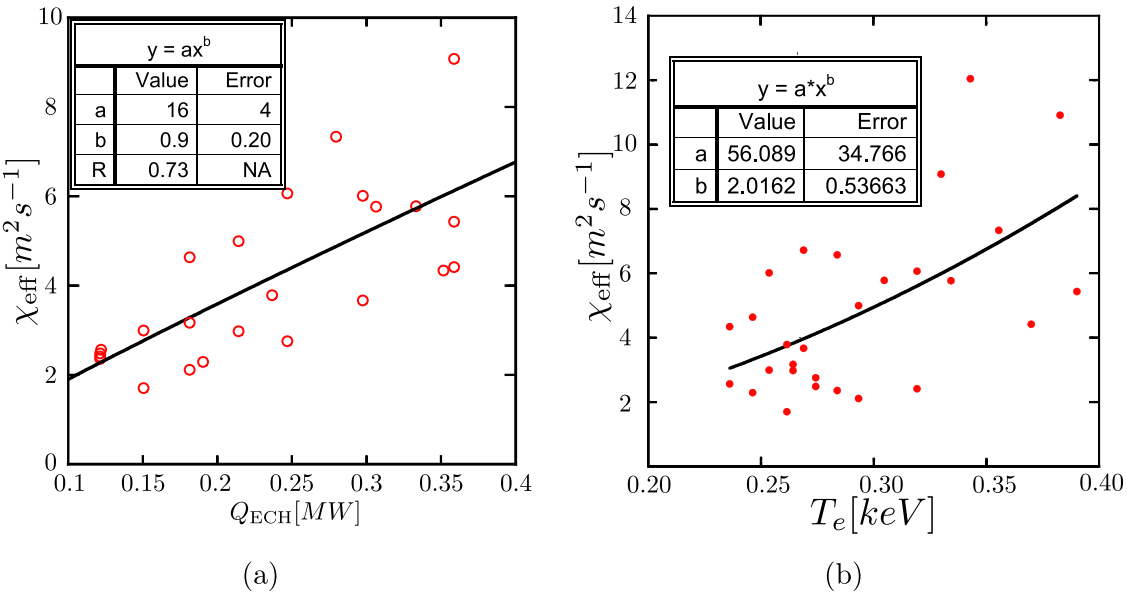

Figure 7. Scaling of χ_e^{eff} with (*a*) Q_{ECH} and (*b*) T_e at $\rho \approx 2/3$ under combined data from boron and lithium wall discharges.

that figures 6(*b*) and 6(*d*) show quite large errors (∼100%) for $\rho \gtrsim 0.8$.

A summary of effective diffusivity behavior is presented in figure 7, where the scattered values of χ_e^{eff} at $\rho = 2/3$ are presented as a function of heating power and local electron temperature. Previous scalings in other stellarators show dependencies of effective diffusivity on heating power and electron temperature around $\rho = 2/3$ of the form $\chi_e \sim Q_{\text{ECH}}^{0.58}$ and $\chi_e \sim T_e^{1.38}$ in LHD [39], $\chi_e \sim Q_{\text{ECH}}^{0.76}$ in the W7-AS semi-local scaling [40], and $\chi_e \sim T_e^{1.52}$ for the Heliotron-E scaling

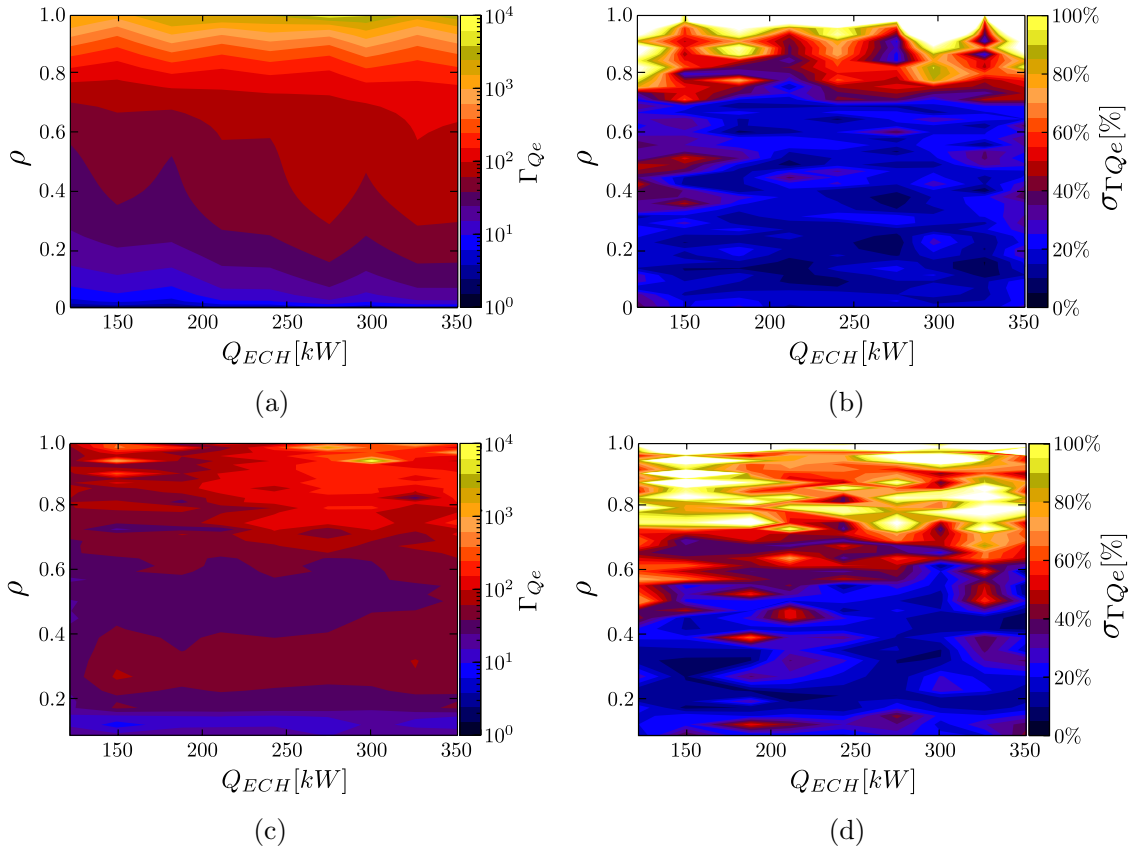

Figure 8. Contour maps of the experimental electron heat fluxes ($m\,s^{-1}$) obtained from the combined set of B- and Li-coated wall discharges (*a*) and neoclassical fluxes for selected Li-coated wall discharges (*c*), as a function of normalized radius and heating power. Figures (*b*) and (*d*) are the respective standard errors presented as a percentage.

[41]. On consideration of the errors, our study shows there is no significant difference between the effective diffusivity under boron or lithium wall conditions. Therefore we have combined the results and for comparison perform a similar investigation of parametric dependencies. In comparison with previous results from other comparable devices, we obtain dependencies of the form $\chi_e^{\rm eff} \sim Q_{\rm ECH}^{0.9\pm0.2}$ and $\chi_e^{\rm eff} \sim T_e^{2\pm0.5}$ around $\rho = 2/3$ (see figure 7). These results confirm and extend the TJ-II previous results [12] and have similarities with those obtained in W7-AS [3, 42, 43].

As our overall documentation of effective electron heat transport in TJ-II ECH discharges we have produced the contour map of experimental fluxes that corresponds to the combined set, B- and Li-coated wall discharges in figure 8(*a*), along with the corresponding percentage errors in figure 8(*b*). Contour maps of the neoclassical fluxes in the lithium cases according to DKES calculations are shown in (*c*) and (*d*) for comparison. The increase in $Q_e^{\rm eff}$ at larger heating powers—larger T_e and smaller collisionality—is a normal feature in the $1/\nu$ collisional regime and is found in both, balance and neoclassical results in the core region. A comparison between the neoclassical heat fluxes and the power balance results under combined boronized and lithiumized wall conditions is presented in figure 9. This shows the percentage of deviation from neoclassical electron heat fluxes as a function of normalized radius ($\rho \geqslant 0.1$) and ECH heating power. The deviation is expressed as the percentage of the

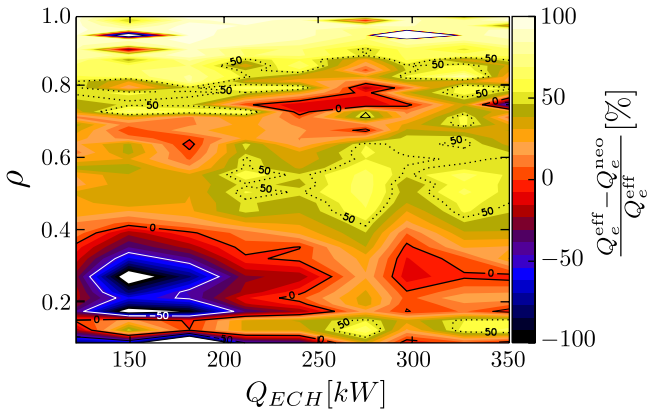

Figure 9. Contour map of percentage of the experimental flux not explained by neoclassical calculations: $100 \times (Q_e^{\rm eff} - Q_e^{\rm neo})/Q_e^{\rm eff}$ under combined boron and lithium wall conditions as a function of normalized radius and heating power. Level lines at 0% and ±50% percentages are plotted with lines.

estimated experimental—balance—fluxes not accounted for by neoclassical theory, so that a value of 0% indicates that the experimental flux is equal to the neoclassical flux, 50% indicates experimental flux is twice the neoclassical theory which can thus account for half the measured flux (observe the dotted level lines on the plot). Values above 70% (i.e. $Q_e^{\rm eff} > 3Q_e^{\rm eff}$) are found only in the edge region. Therefore, even if it cannot be concluded that the experimental fluxes are

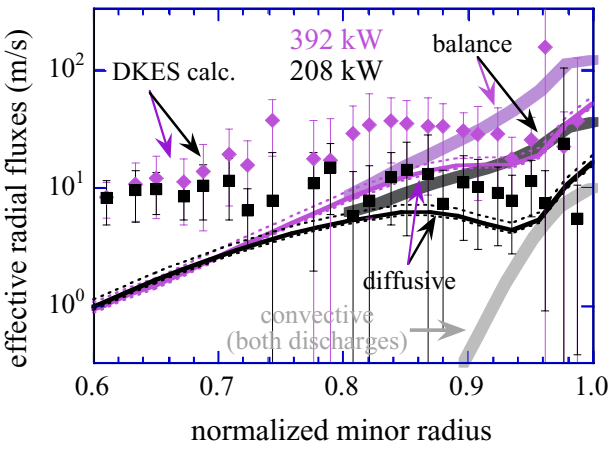

Figure 10. Experimental electron flux profiles for discharges #18455 (392 kW) and #18479 (208 kW) at comparable line averaged density ($\approx 0.6 \times 10^{19}\,\mathrm{m}^{-3}$). Balance calculations are plotted with thin lines corresponding to the diffusive part (see equation (3)) and thick lines when the convective part (thick gray line for $\rho > 0.9$) is added. The values between the dashed lines represent ranges according to errors in the edge electron temperature. Neoclassical calculations are shown with symbols and corresponding error bars.

completely explained by neoclassical transport, the latter can be seen to be important in most of the plasma; excepting the edge region, where neoclassical calculations yield negligible values in comparison with balance estimates. Although the error bars are large in this $\rho > 0.8$ region, the result is common to all mid-size stellarator/heliotron devices: as T_e drops close to the edge, so do the neoclassical fluxes, which cannot then describe the experimental results. It can be also appreciated that the percentage of 'anomaly' in transport increases in the $\rho \sim 0.5$ region with ECH power. We have checked the significance of these results in two ways: firstly, the comparison has been performed between the neoclassical values and the heat balance estimates as obtained from (i) the combined set of boron and lithium discharges (figure 8), (ii) only the lithium set, and (iii) only the Li-coating discharges on which the neoclassical calculations have been performed. The contour plots are quite similar in all cases so we can take figure 8 as representative of the balance-neoclassical comparison. Secondly, we have masked figure 8 where the difference $|Q_e^{\mathrm{eff}} - Q_e^{\mathrm{neo}}|$ is less than the combined error bars to obtain a crude estimate for where we find significant differences between neoclassical calculations and balance estimates. It turns out to be the region where neoclassical values exceed the experimental transport from balance, i.e., the $\rho \lesssim 0.4$, $Q_{\mathrm{ECH}} \lesssim 200\,\mathrm{kW}$ area in figure 9. This corresponds to the power deposition region at low ECH power, where less spread of the heating power density is expected. The core region is subject to uncertainties related with the power deposition profile that have not been considered in this work.

Particle balance has been performed only on the Li-wall cases where He-beam data were available. Figure 10 shows the experimental particle fluxes obtained from equation (3) as $\Gamma_e^{\mathrm{eff}} = L_{n_e}^{-1} D_e^{\mathrm{eff}}$ (lines) and neoclassical calculations (symbols) in the density gradient region of the plasma for the two extreme cases found. Balance estimates include diffusion (thin lines) and a fixed convective part (thick gray line for $\rho > 0.9$), which combine to give the edge balance results shown with thick lines. Dashed lines represent uncertainty in the experimental fluxes due only to T_{ea}. As mentioned in section 3, the smaller Γ^{eff} for the lower power case is not considered significant because there are uncertainties not accounted for, such as the effectiveness of the wall conditioning and, correspondingly, the recycling and gas fueling efficiency. Neoclassical calculations have not been found to be significantly different either. Converting the fluxes to diffusivities (equation (2) for the particle fluxes), particle diffusivities in the density gradient region range between 0.1 and $0.3\,\mathrm{m}^2\,\mathrm{s}^{-1}$, which is smaller than the χ_e^{eff} by at least one order of magnitude. Less of a difference was found, for example, in W7-AS, where D_e was about 0.1–0.3 times χ_e [40].

We see that, within the uncertainties, electron transport in the density gradient region of these ECH plasmas ($0.7 < \rho < 0.9$) is compatible with neoclassical transport expectations excepting, perhaps, the edge plasma. We recall that numerical calculation of ion orbits [19, 34, 44] indicate that convective terms may be discernible in most of TJ-II plasma, but especially near the edge despite the low temperature in this region. The results suggests that the experimental fluxes in the edge region require either some small anomalous contribution or, perhaps, the consideration of collisional non-local effects [45]. The smaller balance values inside $\rho \approx 0.7$ may have to do with underestimated particle sources in the core region; but note also (figure 3) that this is the plasma region where more variability is found between the density gradients.

5. Summary and conclusions

The equivalence of low-Z coatings (Li and B) on the TJ-II chamber wall for the purposes of effective transport profiles in TJ-II ECH plasmas has been documented. The power scan shows that the experimental electron heat fluxes do not change significantly under boron or lithium wall conditioning.

Considering a diffusive description of electron heat transport, ECH plasmas in TJ-II show scalings with heating power and local electron temperature similar to other stellarator/heliotron devices. Effective core diffusivity values are found around 2–3 $\mathrm{m}^2\,\mathrm{s}$, rising with heating power up to 4–5 $\mathrm{m}^2\,\mathrm{s}^{-1}$. Around the mid radius χ_{eff} can reach up to $\approx 10\,\mathrm{m}^2\,\mathrm{s}^{-1}$. In terms of fluxes, the values range from 30 to $90\,\mathrm{m}\,\mathrm{s}^{-1}$ around mid radius under a three-fold increment in ECH power. Comparison with heat fluxes predicted by DKES calculations shows that the neoclassical transport is compatible with the observations in most of the plasma, except maybe for $\rho \gtrsim 0.8$ where the uncertainty is large. In light of the scatter of data this should be interpreted as an indication that non-neoclassical considerations might still be significant (e.g. ECH driven, convection of fast particles) but not dominant in typical ($\bar{n}_e \approx 0.6 \times 10^{19}\,\mathrm{m}^{-3}$) ECH plasmas of the TJ-II stellarator. Effective particle diffusivities in the density gradient region are also found to be compatible with the calculated neoclassical values. Their values are about one order of magnitude smaller than the electron heat diffusivities, giving experimental fluxes in the density gradient regions ($\rho \sim 0.8$) on the order of $10\,\mathrm{m}\,\mathrm{s}^{-1}$.

To the reasonable agreement between balance and neoclassical fluxes, one should add the well-known agreement for the respective radial electric fields, as we knew from previous studies (see e.g. [27] and references therein). Consequently, it is concluded that neoclassical transport mechanisms for the electrons and the electron heat dominate in the main gradient regions of such plasmas. The less well characterized extreme regions (magnetic axis or plasma edge) may still be significantly affected by kinetic effects, like ECH pump-out, or turbulent mechanisms as suggested in predictive calculations based on a local neoclassical treatment [32]. However, it must be recalled that TJ-II is a machine with large effective ripple [28]. Thus, even though local calculations provide a good estimate of the collisional transport of TJ-II (good qualitative agreement with the experiment and, depending on the parameters, reasonable quantitative agreement, see e.g. [27] and references therein), higher-order neoclassical effects (e.g. [34, 45]) may be relevant for an accurate quantitative description under some circumstances. In particular, they could improve the agreement with the experiment at the near edge region.

Acknowledgments

This work has been developed in a collaboration frame between Ciemat (*Centro de Investigaciones Energéticas, Medio-Ambientales y Tecnológicas, Madrid, Spain*) and the ITCR (*Instituto Tecnológico de Costa Rica, Cartago, Costa Rica*); and has been partially supported by the *Ministerio de Ciencia y Tecnología de Costa Rica* and the Vicerectory of Research and Extension (ITCR) through the project number 5402-1450-0901.

References

[1] Yamada H *et al* 2005 *Nucl. Fusion* **45** 1684
[2] Lyon J F 1990 *Plasma Phys. Control. Fusion* **32** 1041
[3] Stroth U 1998 *Plasma Phys. Control. Fusion* **40** 9
[4] Yokoyama M. *et al* 2007 *Nucl. Fusion* **47** 1213
[5] Baldzuhn J, Kick M, Maassberg H and The W7-AS Team 1998 *Plasma Phys. Control. Fusion* **40** 967
[6] Dinklage A *et al* 2013 *Nucl. Fusion* **53** 063022
[7] Maassberg H *et al* 1993 *Plasma Phys. Control. Fusion* **35** B319–32
[8] Ascasíbar E, Estrada T, Castejón F, López-Fraguas A, Pastor I, Sánchez J, Stroth U, Qin J and The TJ-II Team 2005 *Nucl. Fusion* **45** 276
[9] Tabarés F L *et al* and The TJ-II Team 2008 *Plasma Phys. Control. Fusion* **50** 124051
[10] Sánchez J *et al* 2009 *Nucl. Fusion* **49** 104018
[11] Tabarés F L *et al* and The Team TJ II 2010 *Contrib. Plasma Phys.* **50** 610–5
[12] Vargas V I, López-Bruna D, Herranz J, Castejón F and The TJ-II Team 2007 *Nucl. Fusion* **47** 1367
[13] Castejón F, Tribaldos V, García-Cortés I, de la Luna E, Herranz J, Pastor I, Estrada T and The Team TJ II 2002 *Nucl. Fusion* **42** 271
[14] Kick M, Maaßberg H, Anton M, Baldzuhn J, Endler M, Görner C, Hirsch M, Weller A, Zoletnik S and The W7-AS Team 1999 *Plasma Phys. Control. Fusion* **41** A549
[15] Maassberg H, Beidler C D, Gasparino U, Dyabilin K S, Marushchenko N B, Murakami S and The W7-AS Team 2000 *Phys. Plasmas* **7** 295–311
[16] Ochando M A, Medina F and The TJ-II Team 2003 *Plasma Phys. Control. Fusion* **45** 221
[17] Castejón F *et al* 2004 *Nucl. Fusion* **44** 593
[18] Estrada T *et al* 2004 *Plasma Phys. Control. Fusion* **46** 277
[19] Vargas V I *et al* 2009 Density dependence of particle transport in ECH plasmas of the TJ-II stellarator *Technical Report* 1162 Ciemat Madrid, Spain
[20] Herranz J *et al* 2003 *Fusion Eng. Des.* **65** 525
[21] Hidalgo A *et al* 2004 *Rev. Sci. Instrum.* **75** 3478
[22] van Milligen B P, Estrada T, Ascasibar E, Tafalla D, Lopez-Bruna D, Fraguas A L, Jimenez J A, Garcia-Cortes I, Dinklage A and Fischer R 2011 *Rev. Sci. Instrum.* **82** 073503
[23] Fontdecaba J M, Balbin R, Petrov S and The TJ-II Team 2003 Charge-exchange neutral particle analyzer diagnostic of TJ-II *Technical Report* 1014 Ciemat Madrid, Spain
[24] Guzmán F, Tabarés F L, Tafalla D, García-Cortés I and Balbín R 2009 *J. Nucl. Mater.* **390–391** 1127–30
[25] Fontdecaba J M, Pastor I, Arévalo J, Herranz J, McCarthy K J and Sánchez-Burillo G 2010 *Plasma Fusion Res.* **5** S2085
[26] Melnikov A V *et al* 2011 *Nucl. Fusion* **51** 083043
[27] Velasco J L, Alonso J A, Calvo I, Arévalo J, Sánchez E, Eliseev L, Perfilov S, Estrada T, López-Fraguas A, Hidalgo C and the TJ-II Team 2013 *Plasma Phys. Control. Fusion* **55** 124044
[28] Velasco J L and Castejón F 2012 *Plasma Phys. Control. Fusion* **54** 015005
[29] Hirshman S P, Shaing K C, van Rij W I, Beasley C O and Crume E C 1986 *Phys. Fluids* **29** 2951–9
[30] Pereverzev G V and Yushmanov P N 2002 ASTRA automated system for transport analysis *Technical Report* IPP 5/98 Max Plank Institut für Plasmaphysik, Garching
[31] Eguilior S, Castejón F, de la Luna E, Cappa A, Likin K, Fernández A and The Team TJ II 2003 *Plasma Phys. Control. Fusion* **45** 105
[32] Turkin Y, Beidler C D, Maaßberg H, Murakami S, Tribaldos V and Wakasa A 2011 *Phys. Plasmas* **18** 022505
[33] Reiter D 2005 The EIRENE code user manual (including: B2-EIRENE interface) www.eirene.de/html/manual.html
[34] Tribaldos V and Guasp J 2005 *Plasma Phys. Control. Fusion* **47** 545
[35] Vargas V I, López-Bruna D and Herranz F C J 2006 *Informes Técnicos Ciemat* **1079** (www–fusion.ciemat.es/InternalReport/IR1079.pdf)
[36] Tabarés F L, Brañas B, García-Cortés I, Tafalla D, Estrada T and Tribaldos V 2001 *Plasma Phys. Control. Fusion* **43** 1023
[37] Canik J M, Anderson D T, Anderson F S B, Clark C, Likin K M, Talmadge J N and Zhai K 2007 *Phys. Plasmas* **14** 056107
[38] Volkov E D *et al* 1993 *(Proc. 14th Int. Conf. on Plasma Physics and Controlled Nuclear Fusion Research (Würzburg, Germany, 1992)* vol 2 (Vienna: IAEA) p 679
[39] Yamazaki K and Amano T 1992 *Nucl. Fusion* **32** 633–44
[40] Ringler H, Gasparino U, Kuhner G, Maassberg H, Renner H and Sardei F 1990 *Plasma Phys. Control. Fusion* **32** 933
[41] Sano F *et al* 1990 *Nucl. Fusion* **30** 81
[42] Stroth U *et al* 1995 *Phys. Scr.* **51** 655
[43] Brakel R *et al* 1997 *Plasma Phys. Control. Fusion* **39** B273
[44] Velasco J L, Castejon F and Tarancon A 2009 *Phys. Plasmas* **16** 052303
[45] Satake S, Okamoto M, Nakajima N, Sugama H and Yokoyama M 2006 *Plasma Fusion Res.* **1** 002